*Supplementary Materials*

# Stimuli-Responsive Rifampicin-Based Macromolecules

(a)



(b)
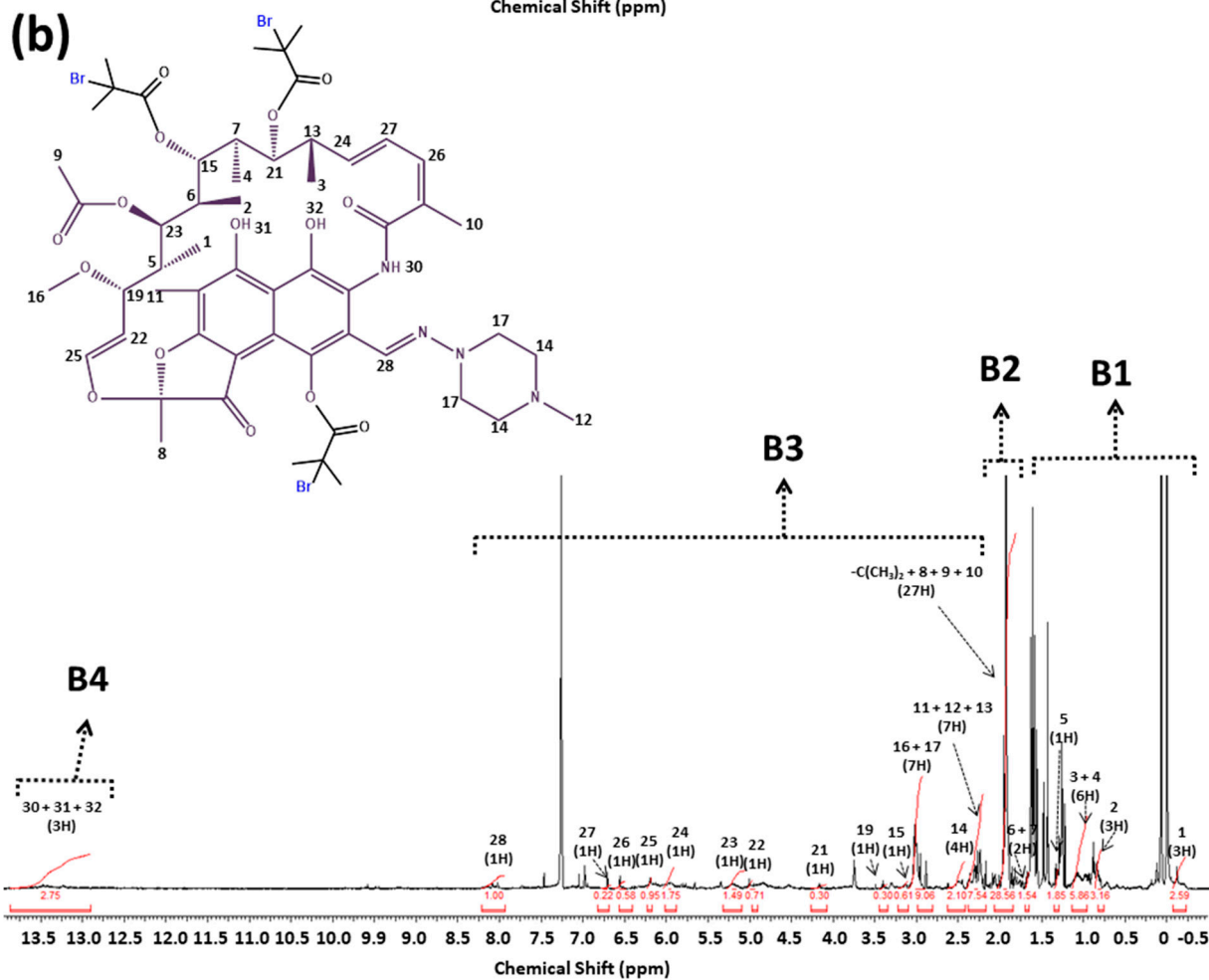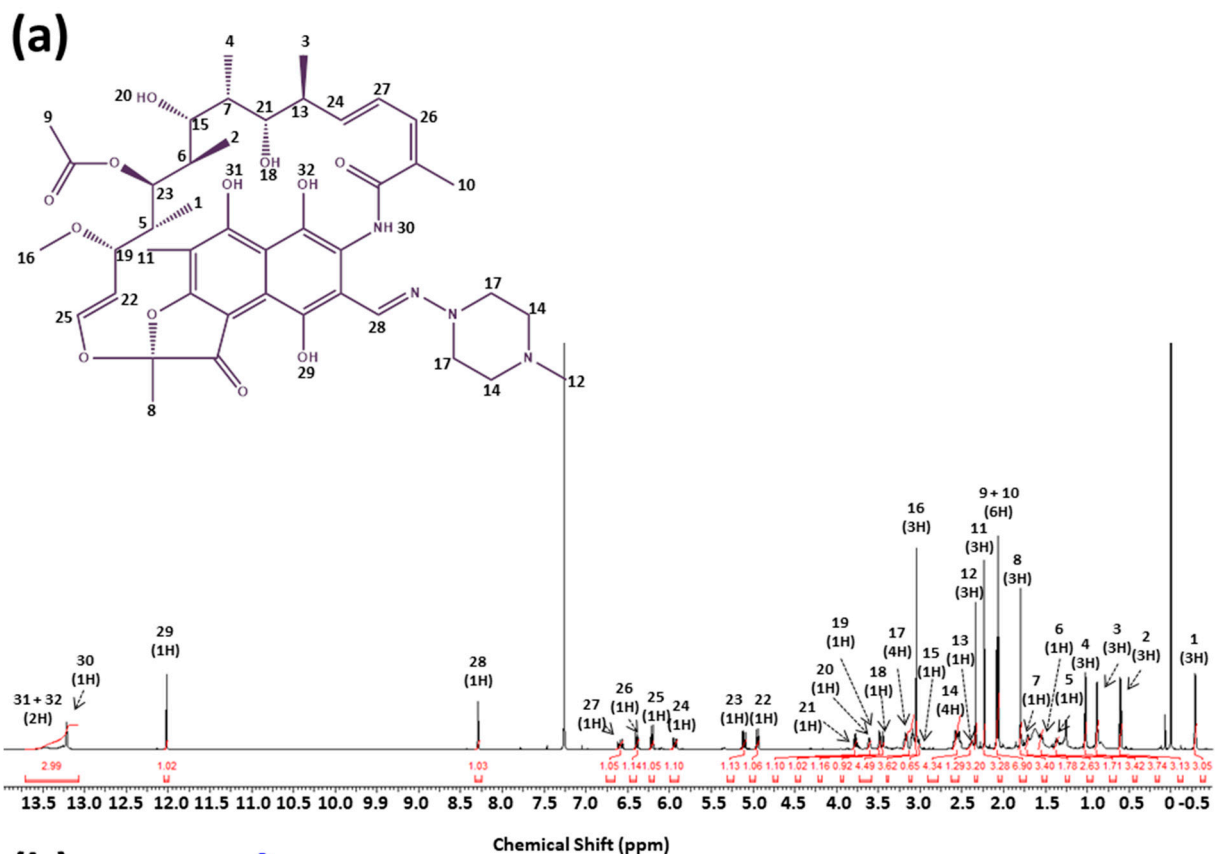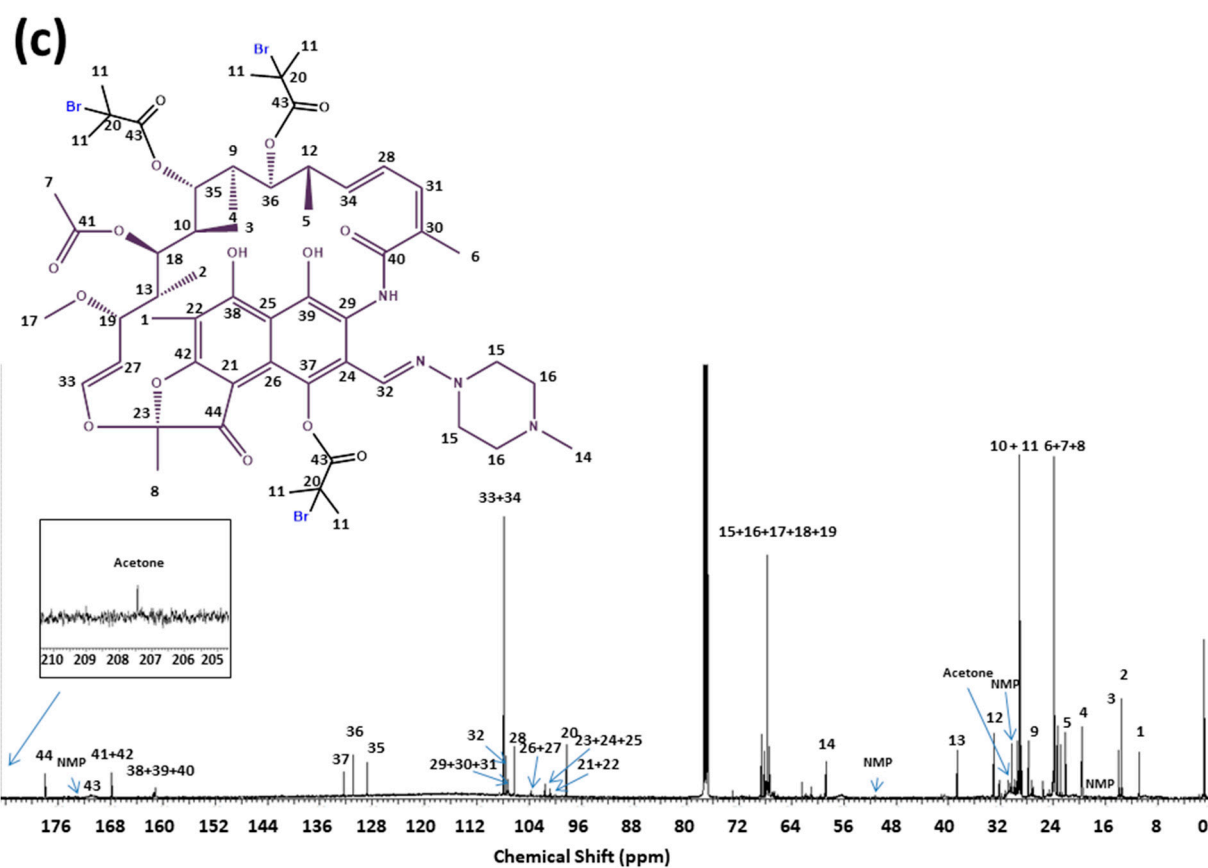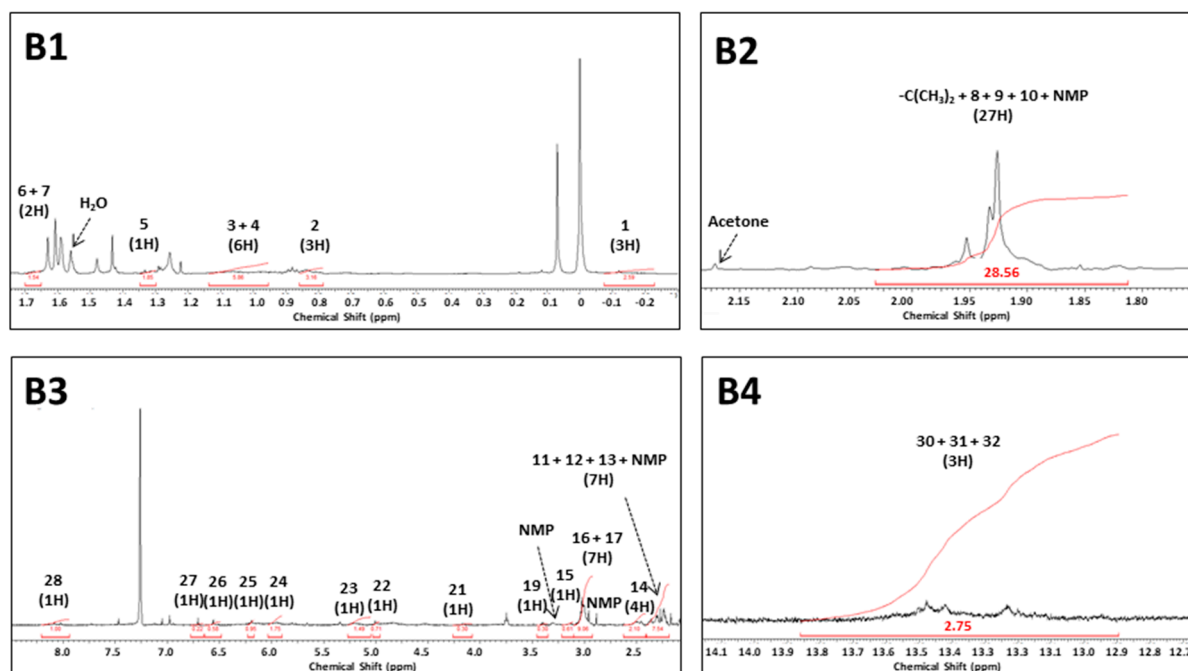
**Figure S1.** $^1$H NMR of (**a**) rifampicin (CDCl$_3$); (**b**) $^1$H NMR and (**c**) $^{13}$C NMR of Rif-Br$_3$ supramolecular initiator ($M_n$ = 1269.94, $Đ$ = 1.19) after purification (CDCl$_3$).
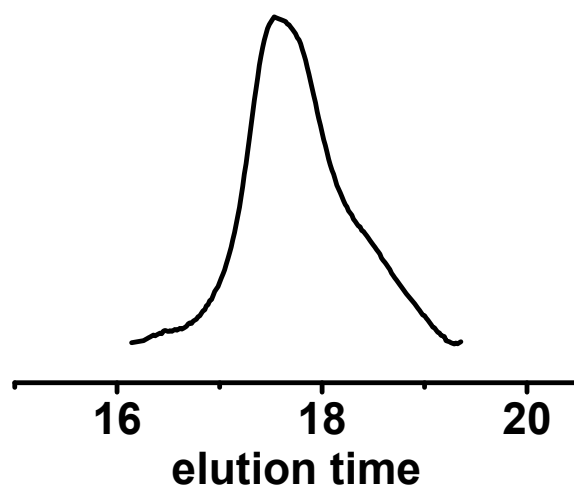
**Figure S2.** GPC trace of Rif-Br$_3$ macroinitiator.
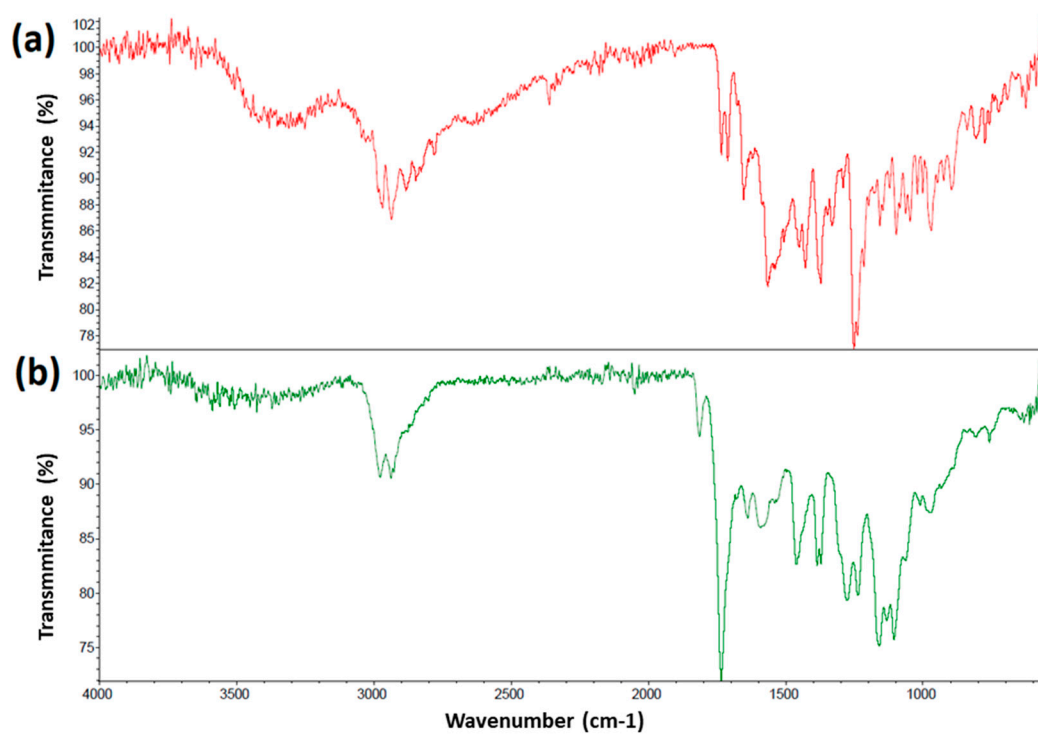


**Figure S3.** FT-IR characterization of (**a**) rifampicin and (**b**) Rif-Br$_3$ macroinitiator.
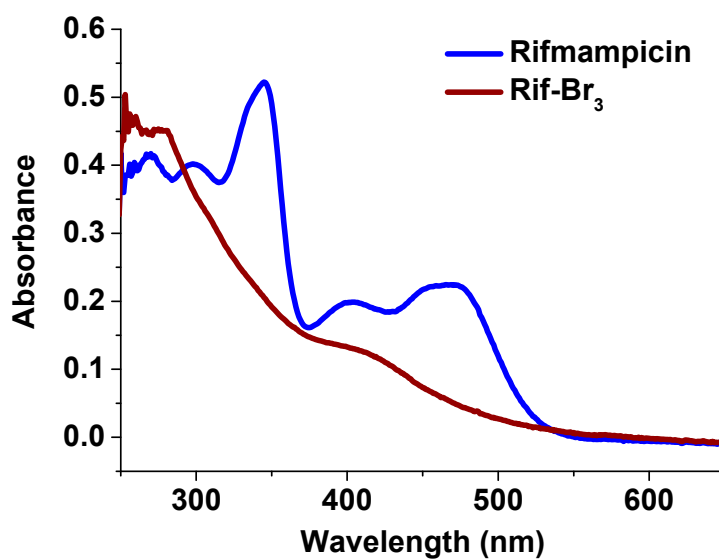
**Figure S4.** UV-vis spectrum of rifampicin and Rif-Br₃ macroinitiator in THF.
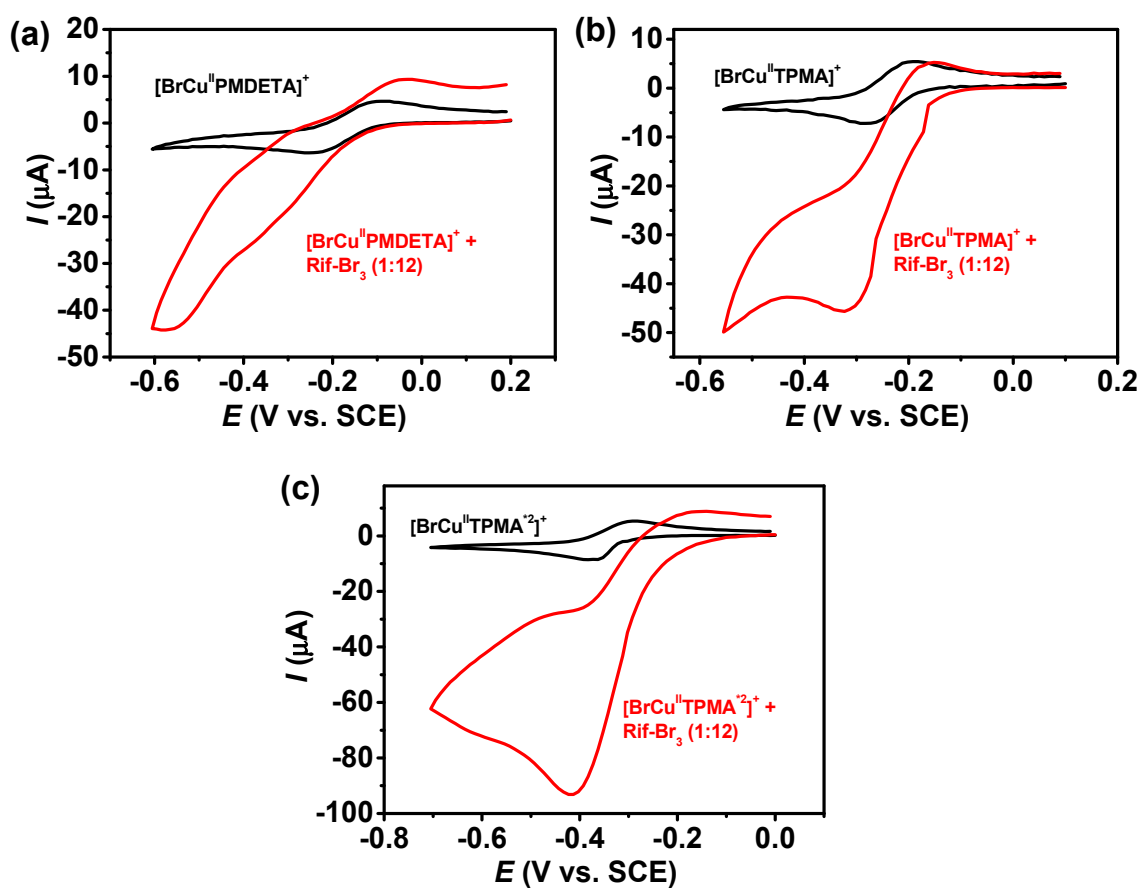


**Figure S5.** Cyclic voltammogram of 0.8 mM $Cu^{II}Br_2$/L in DMF containing 0.2 M TBAP in the absence (black line) and in the presence of 9.8 mM Rif-Br₃ (red line) recorded at v = 0.1 V·s⁻¹, where L (ligand) is (**a**) PMDETA, (**b**) TPMA and (**c**) TPMA*².
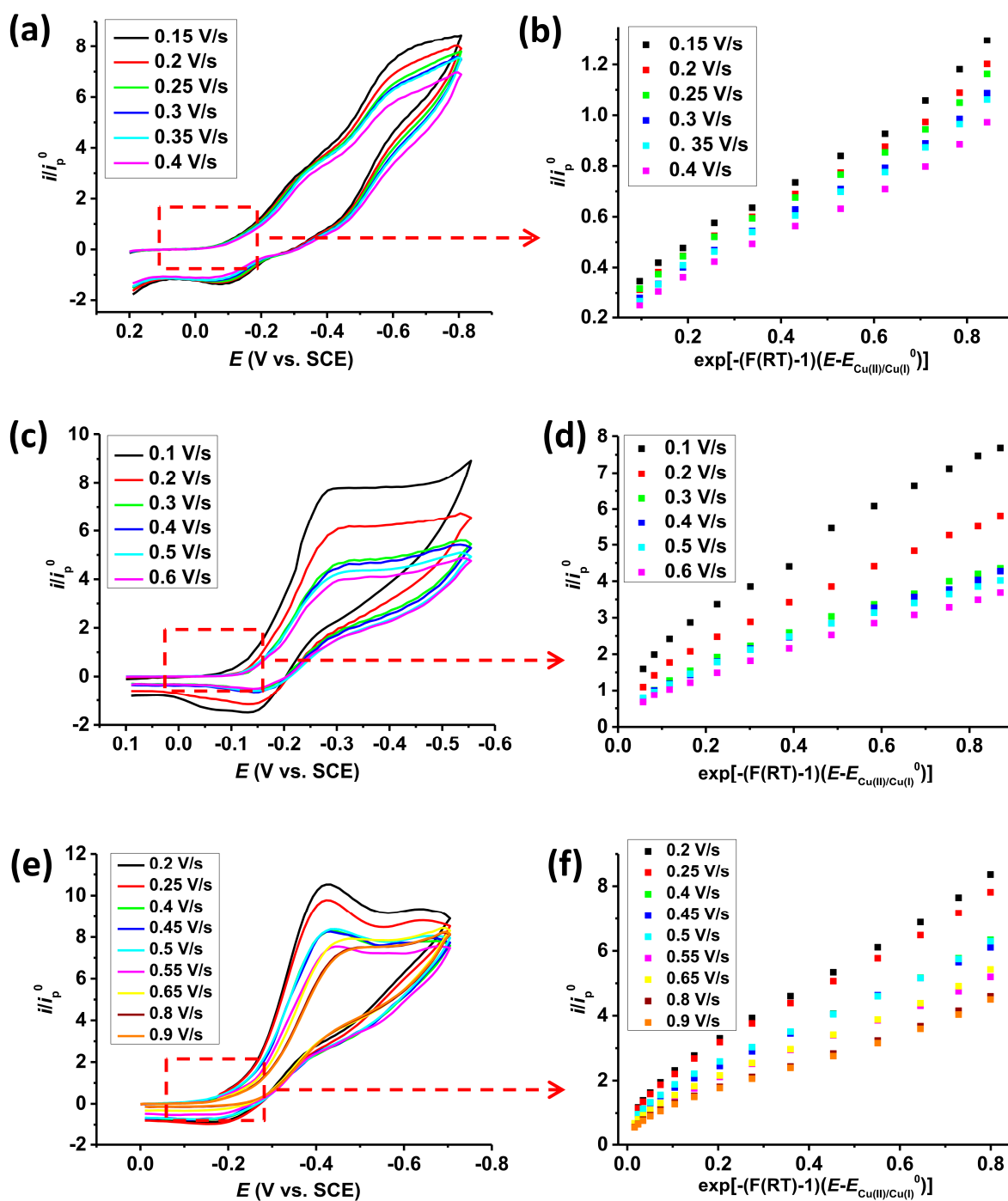
**Figure S6.** Cyclic voltammograms of 0.8 mM $Cu^{II}Br_2/L$ in DMF recorded at a different scan rates (given next to the curves) in the presence of 9.8 mM Rif-Br$_3$ (3 Br molecules) and 39.9 mM TEMPO; the current was normalized with respect to the peak current ($i_P^0$) recorded in the absence of Rif-Br$_3$, where L (ligand) is (**a**) PMDETA, (**c**) TPMA and (**e**) TPMA$^{*2}$; Foot-of-the-wave analysis of the catalytic peak to determine $k_a$, the slope $a$ of the plots of $i/i_P°$ vs. exp[-$F(E-E_{Cu(II)/Cu(I)}^0)/RT$]: $a = 2.24\sqrt{\frac{k_a C_A^0 RT}{Fv}}$, where $i$—catalytic current, $i_P^0$—reversible one-electron reduction of the copper catalyst complex in the absence of Rif-Br$_3$, $C_A^0$—initial Rif-(P$n$BA-Br)$_3$ concentration, $F$—Faraday constant, $R$—gas constant, $T$ = 298 K, $E_{Cu^{II}/Cu^I}^0$ is the half wave potential of the $Cu^{II}Br_2/L$, using (**b**) PMDETA, (**d**) TPMA and (**e**) TPMA$^{*2}$ as a ligand.
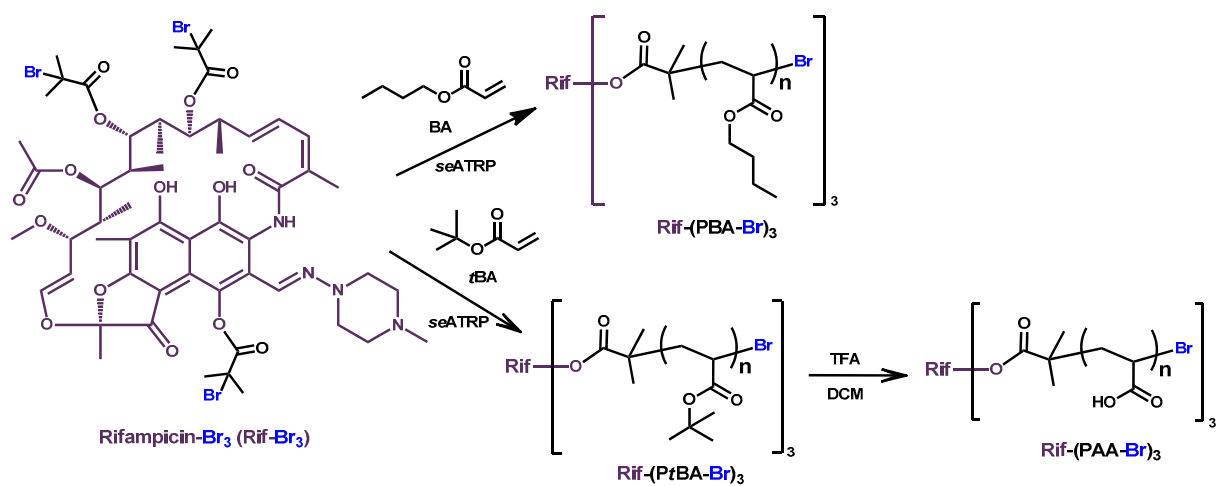
**Figure S7.** Synthetic route for the preparation of rifampicin-based macromolecules with acrylates (P*n*BA and P*t*BA) and poly(acrylic acid) (PAA) side chains.
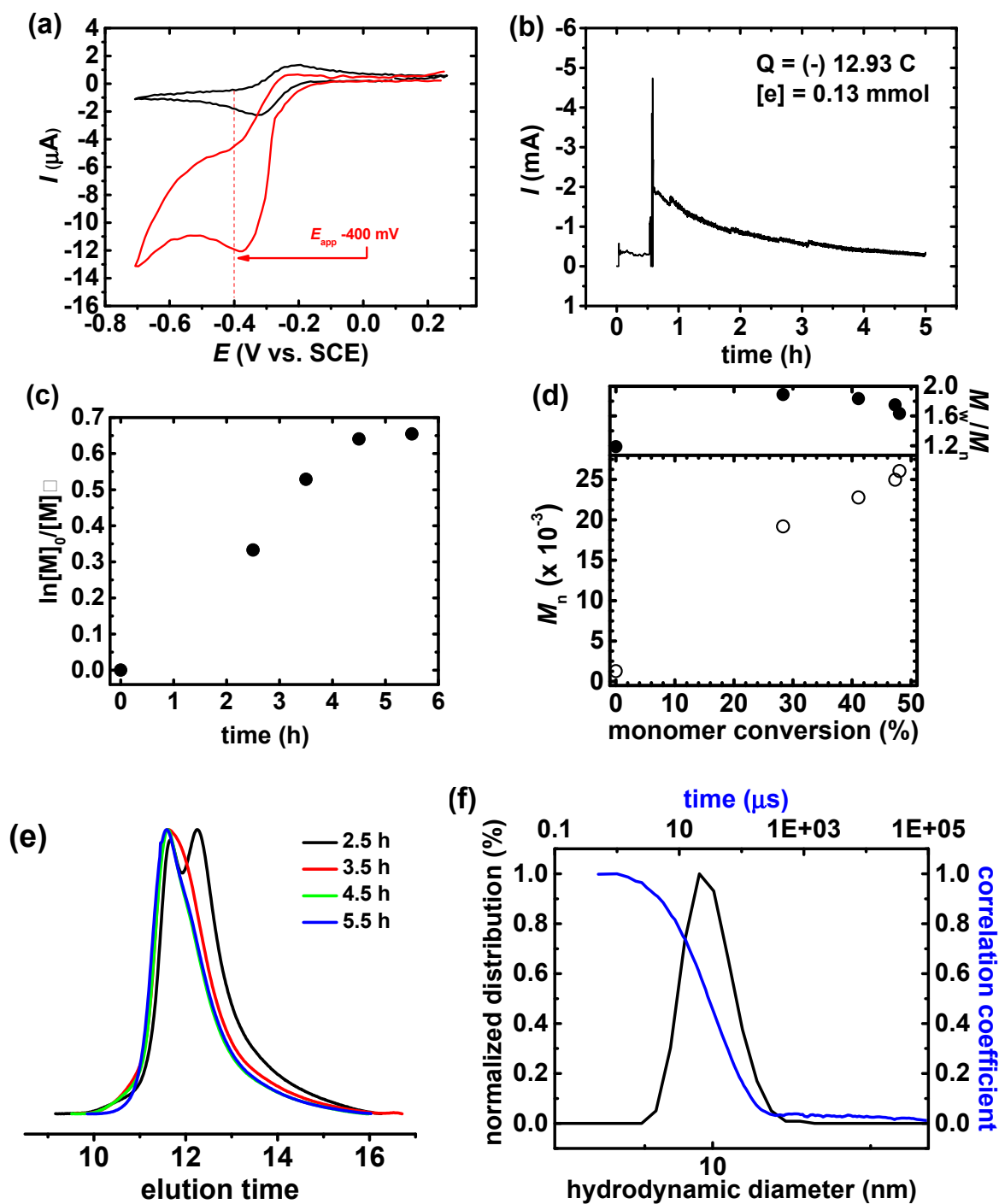
**Figure S8.** (**a**) Cyclic voltammogram of 0.44 mM $Cu^{II}Br_2$/TPMA*2 in 15% (*v/v*) *n*BA/DMF ([*n*BA]$_0$ = 1.10 M) containing 0.2 M TBAP in the absence (black line) and in the presence of 1.35 mM Rif-Br$_3$ (red line) recorded at *v* = 0.1 V·s$^{-1}$, (**b**) current profile vs. time for the polymerization of *n*BA from Rif-Br$_3$, (**c**) First-order kinetic plot of monomer conversion vs. time, (**d**) $M_n$ and $M_w/M_n$ vs. monomer conversion, (**e**) GPC traces of *n*BA polymerization and their evolution over reaction time, (**f**) DLS hydrodynamic size distributions by volume of Rif-(P*n*BA-Br)$_3$. Table 1, entry 1.
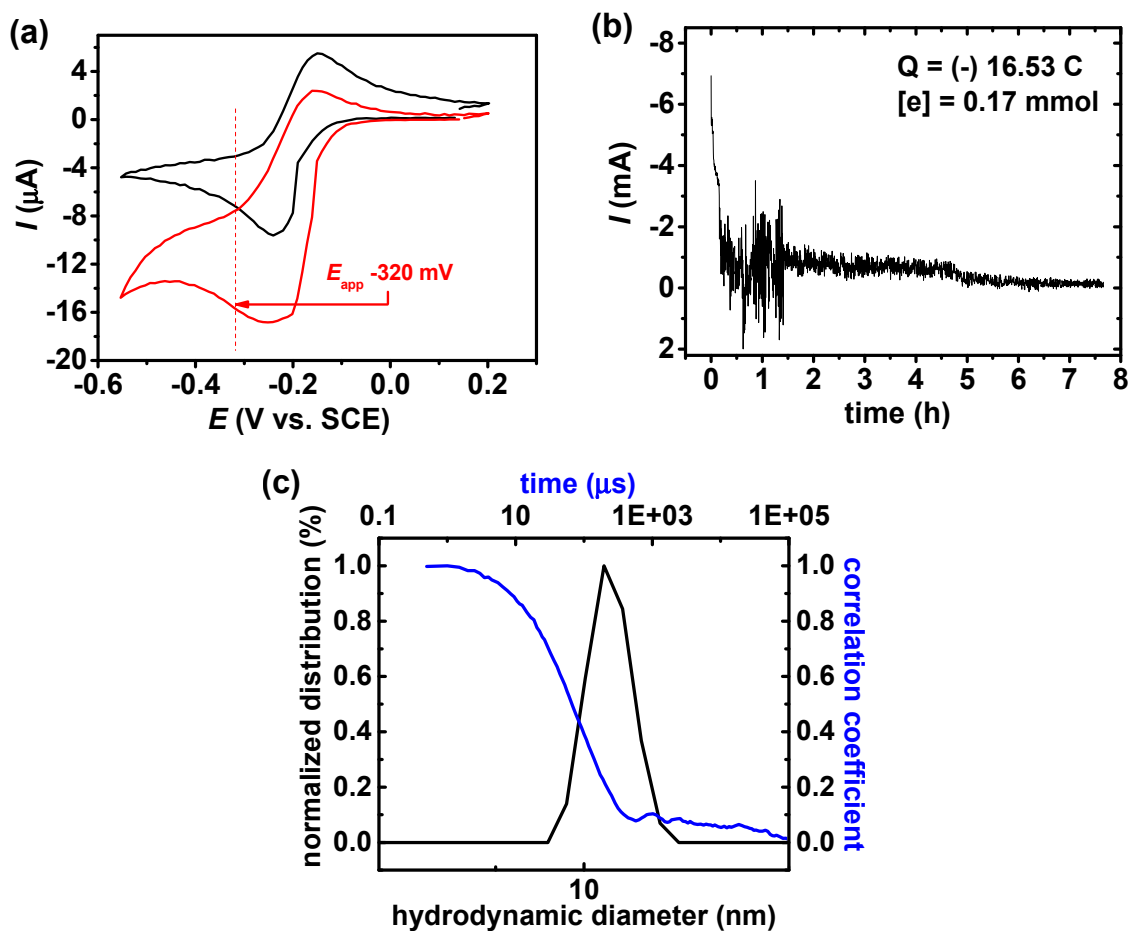
**Figure S9.** (**a**) Cyclic voltammogram of 0.88 mM $Cu^{II}Br_2$/TPMA in 30% (*v/v*) *n*BA/DMF ([*n*BA]$_0$ = 2.19 M) containing 0.2 M TBAP in the absence (black line) and in the presence of 2.71 mM Rif-Br$_3$ (red line) recorded at *v* = 0.1 V·s$^{-1}$, (**b**) current profile vs. time for the polymerization of *n*BA from Rif-Br$_3$, (**c**) DLS hydrodynamic size distributions by volume of Rif-(P*n*BA-Br)$_3$. Table 1, entry 2.
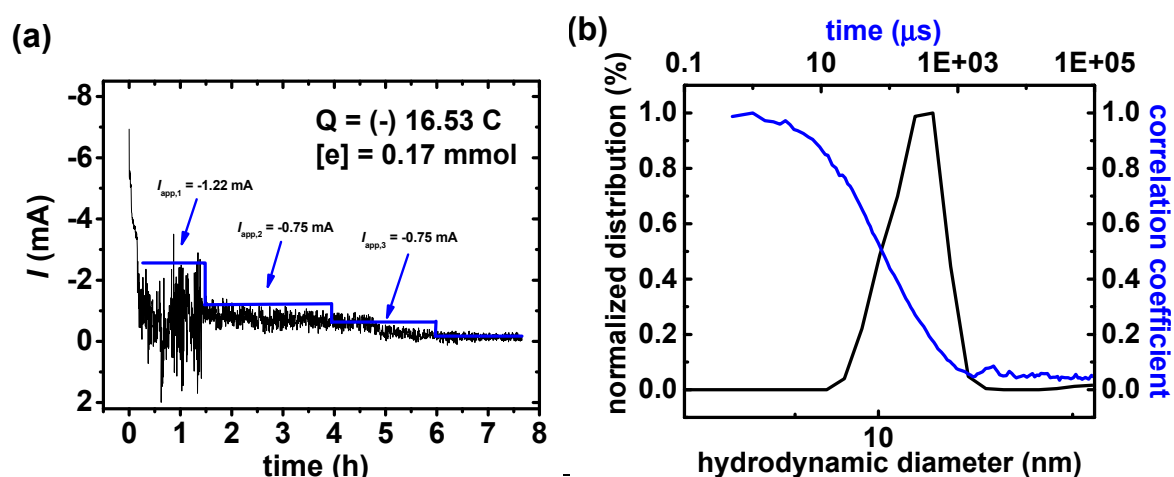


**Figure S10.** (**a**) Current profile vs. time for the polymerization of *n*BA from Rif-Br$_3$ under constant potential conditions and the determined current steps for constant current electrolysis (**b**) DLS hydrodynamic size distributions by volume of Rif-(P*n*BA-Br)$_3$. Table 1, entry 3.
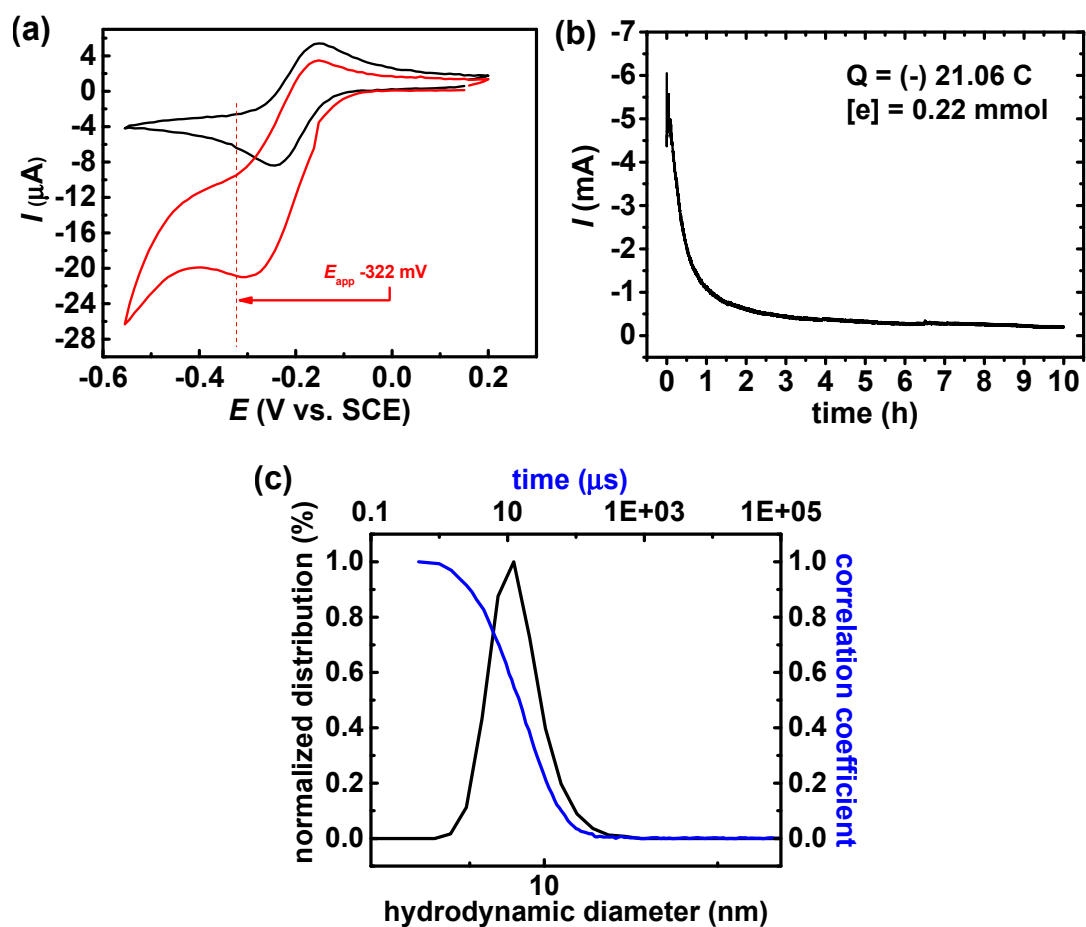
**Figure S11.** (**a**) Cyclic voltammogram of 0.82 mM $Cu^{II}Br_2$/TPMA in 30% (v/v) *t*BA/DMF ([*t*BA]$_0$ = 2.05 M) containing 0.2 M TBAP in the absence (black line) and in the presence of 6.74 mM Rif-Br$_3$ (red line) recorded at $v$ = 0.1 V·s$^{-1}$, (**b**) current profile vs. time for the polymerization of *t*BA from Rif-Br$_3$, (**c**) DLS hydrodynamic size distributions by volume of Rif-(P*t*BA-Br)$_3$. Table 1, entry 4.
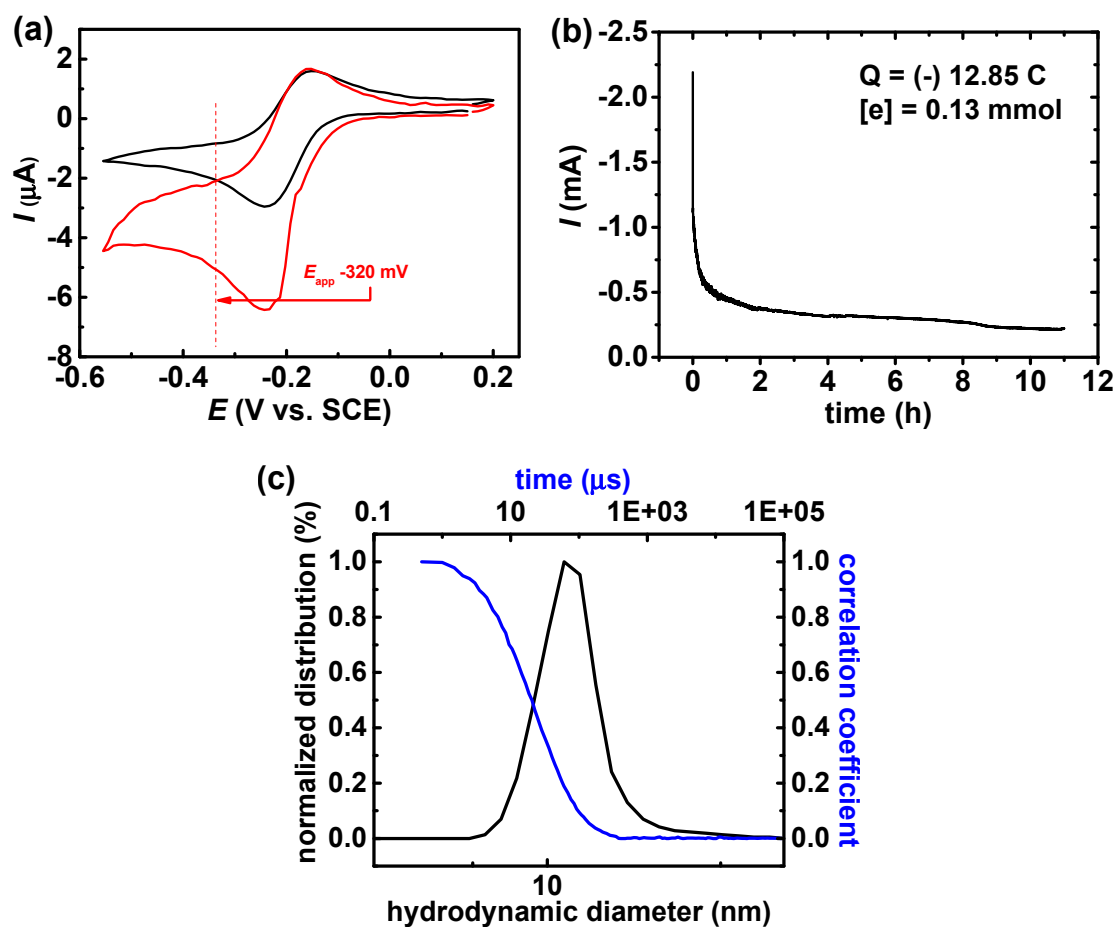
**Figure S12.** (**a**) Cyclic voltammogram of 0.43 mM $Cu^{II}Br_2$/TPMA in 16% (v/v) *t*BA/DMF ($[tBA]_0$ = 1.07 M) containing 0.2 M TBAP in the absence (black line) and in the presence of 1.95 mM Rif-(P*t*BA-Br)$_3$ (red line) recorded at $v$ = 0.1 V·s$^{-1}$, (**b**) current profile vs. time for the polymerization of *t*BA from Rif-(P*t*BA-Br)$_{3,}$ (**c**) DLS hydrodynamic size distributions by volume of Rif-(P*t*BA-*b*-P*t*BA-Br)$_3$. Table 1, entry 5.
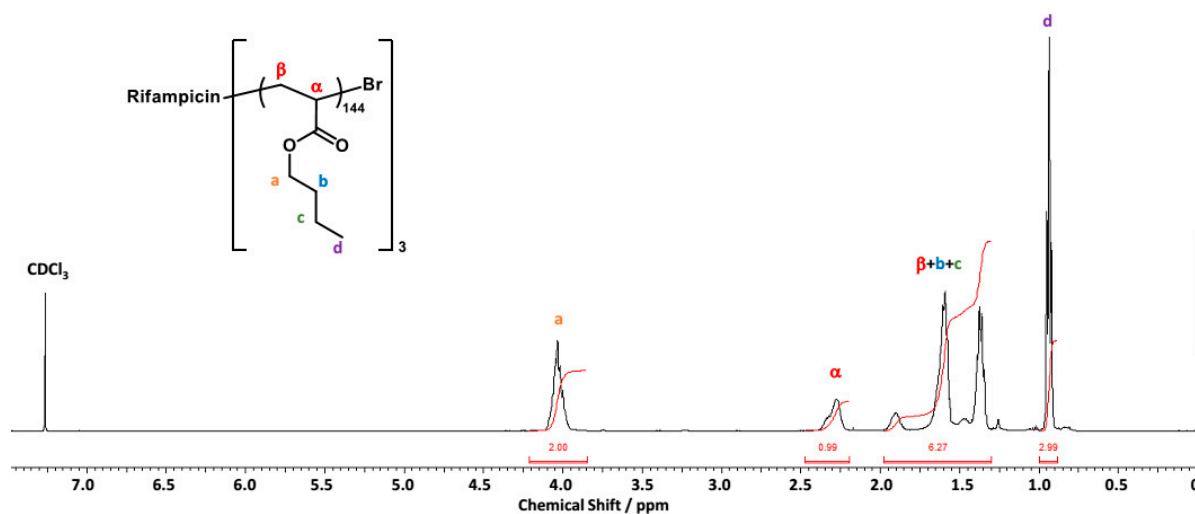


**Figure S13.** $^1$H NMR spectrum of Rif-(P*n*BA-Br)$_3$ polymers ($M_n$ = 56100, *Đ* = 1.59) after purification (in CDCl$_3$). Table 1, entry 3.
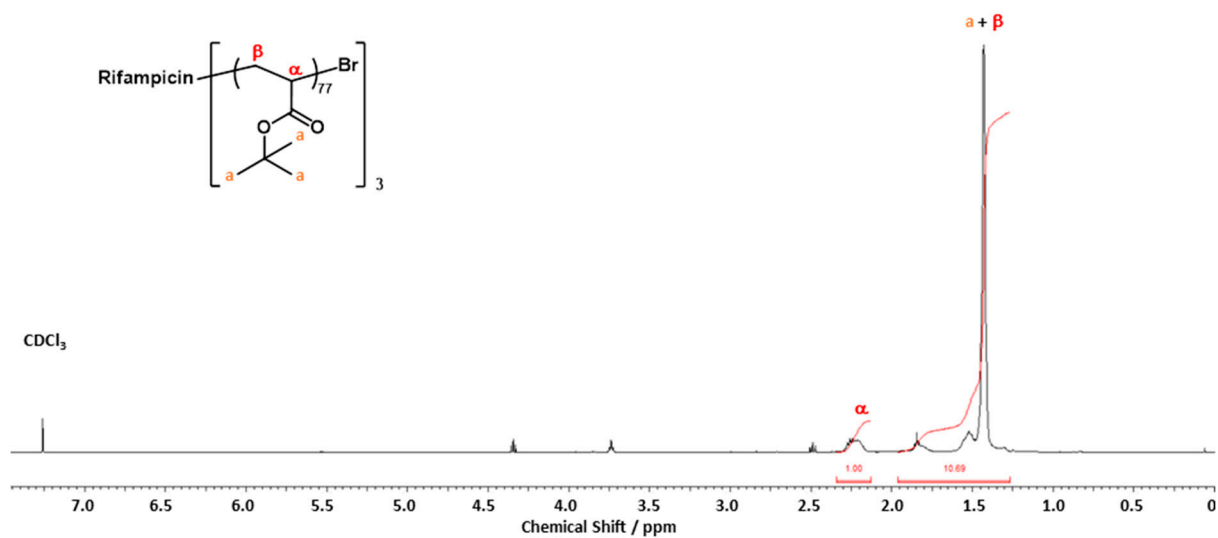
**Figure S14.** $^1$H NMR spectrum of Rif-(P$t$BA-Br)$_3$ polymers ($M_n$ = 30100, Đ = 1.71) after purification (in CDCl$_3$). Table 1, entry 4.
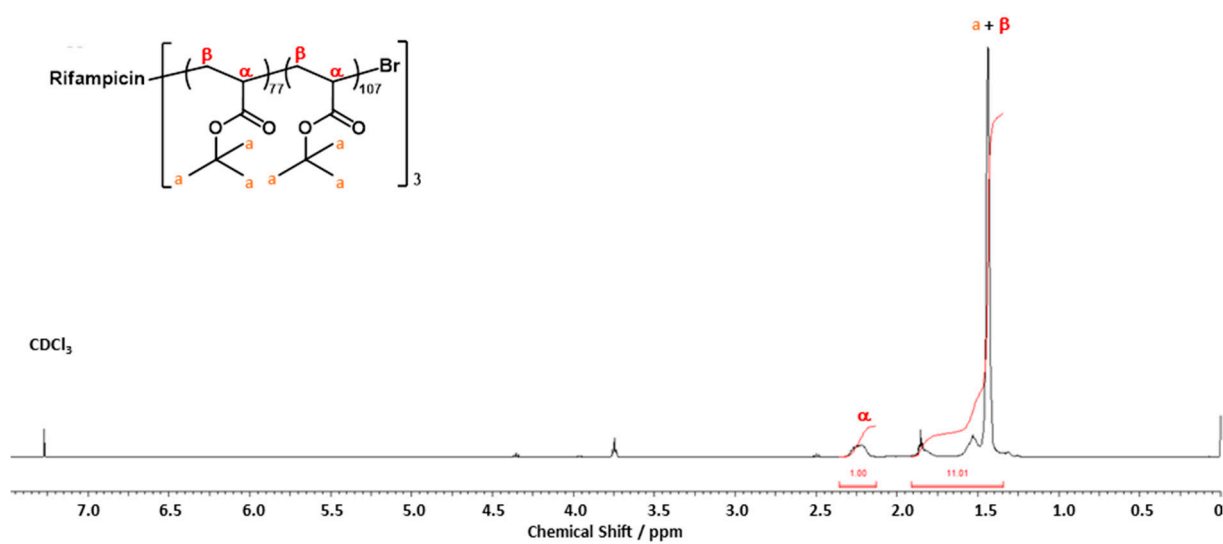


**Figure S15.** $^1$H NMR spectrum of Rif-(P$t$BA-$b$-P$t$BA-Br)$_3$ polymers ($M_n$ = 72100, Đ = 1.58) after purification (in CDCl$_3$). Table 1, entry 5.
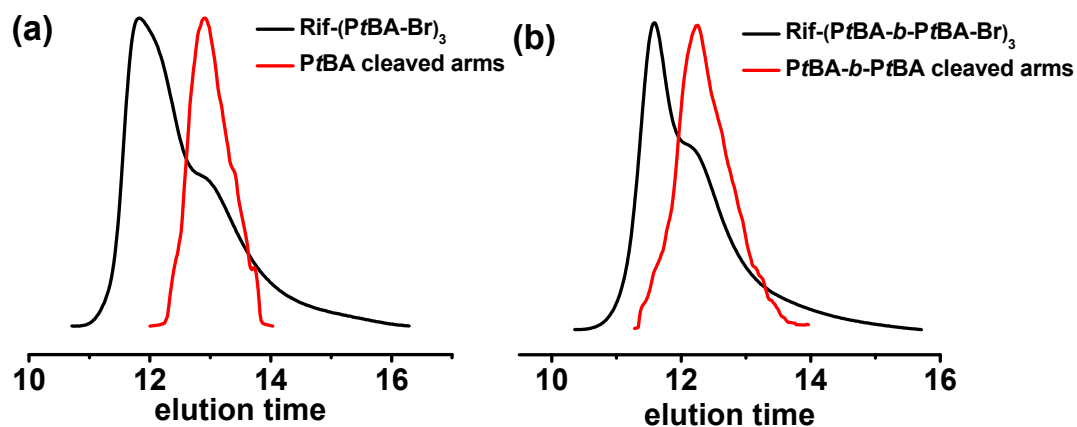
**Figure S16.** GPC traces of (**a**) Rif-(P*t*BA-Br)₃ (Table 1, entry 4) and the corresponding cleaved P*t*BA arms, and (**b**) Rif-(P*t*BA-*b*-P*t*BA-Br)₃ (Table 1, entry 5) and the corresponding cleaved P*t*BA-*b*-P*t*BA arms.
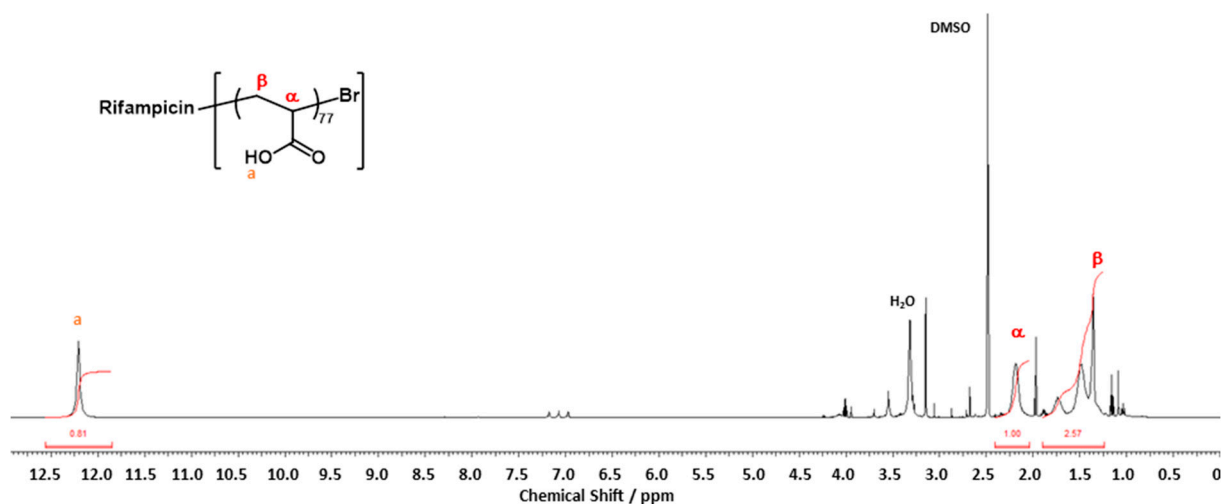


**Figure S17.** ¹H NMR spectrum of Rif-(PAA-Br)₃ polymers after purification (in DMSO-*d*₆). Table 1, entry 4.
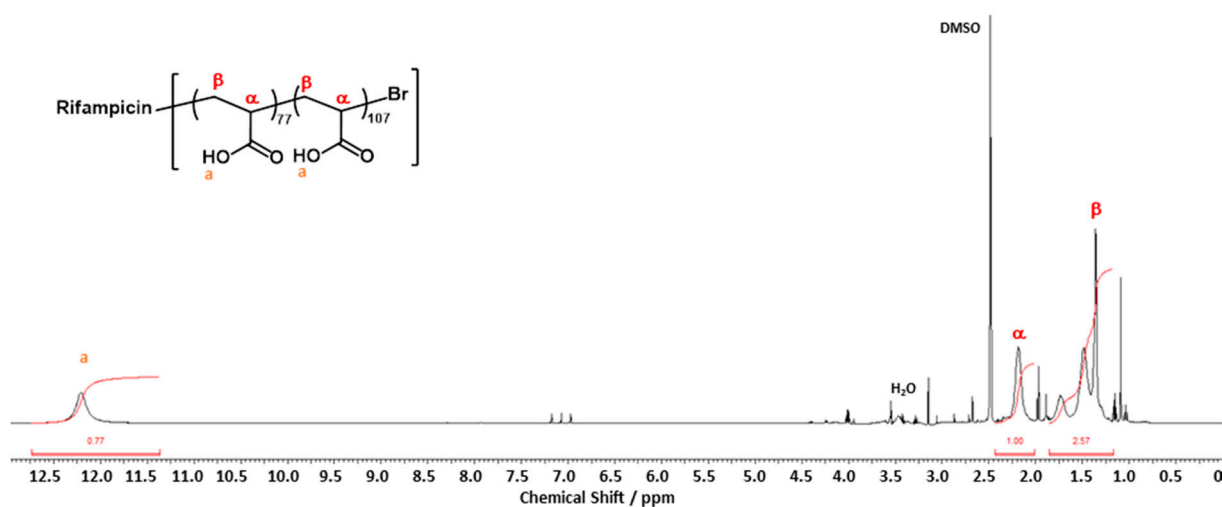


**Figure S18.** ¹H NMR spectrum of Rif-(PAA-*b*-PAA-Br)₃ polymers after purification (in DMSO-*d*₆). Table 1, entry 5.
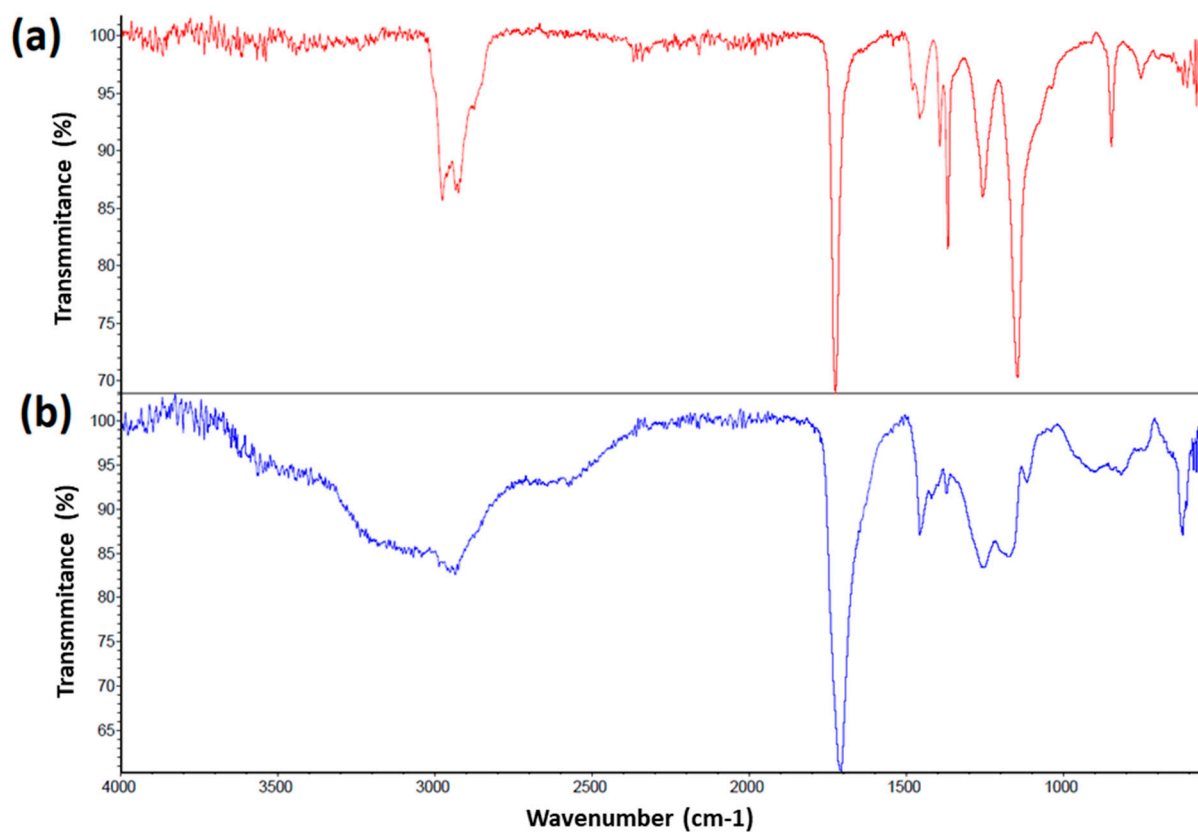
**Figure S19.** FT-IR characterization of (**a**) Rif-(P*t*BA-Br)₃ (Table 1, entry 4) and (**b**) Rif-(PAA-Br)₃.
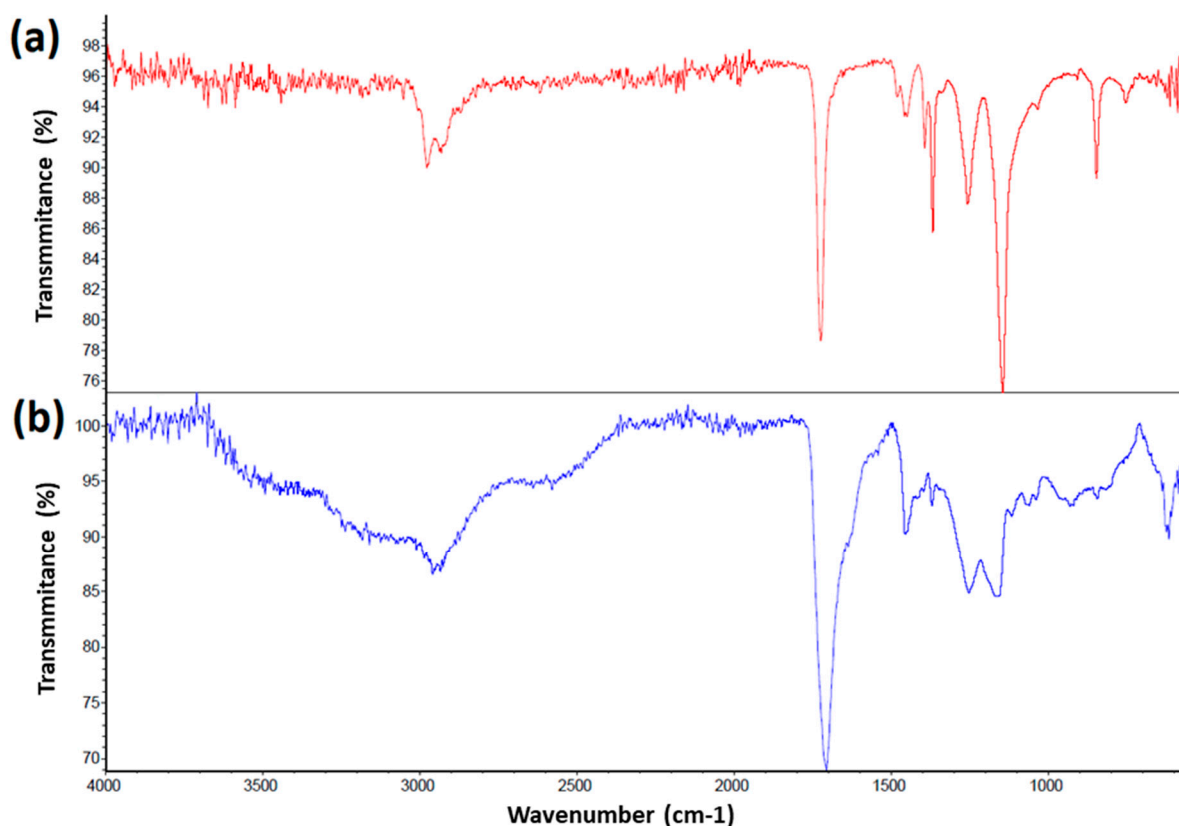


**Figure S20.** FT-IR characterization of (**a**) Rif-(P*t*BA-*b*-P*t*BA-Br)₃ (Table 1, entry 5) and (**b**) Rif-(PAA-*b*-PAA-Br)₃.
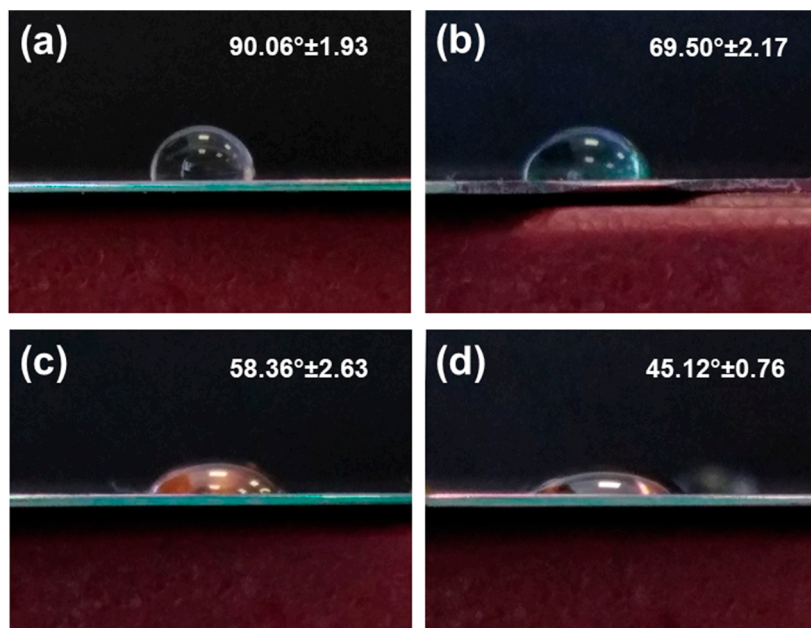
**Figure S21.** Water contact angle images of (a) Rif-(P*t*BA-Br)₃ (Table 1, entry 4) and (b) corresponding Rif-(PAA-Br)₃, and diiodomethane contact angle images of (c) Rif-(P*t*BA-Br)₃ (Table 1, entry 4) and (d) corresponding Rif-(PAA-Br)₃.
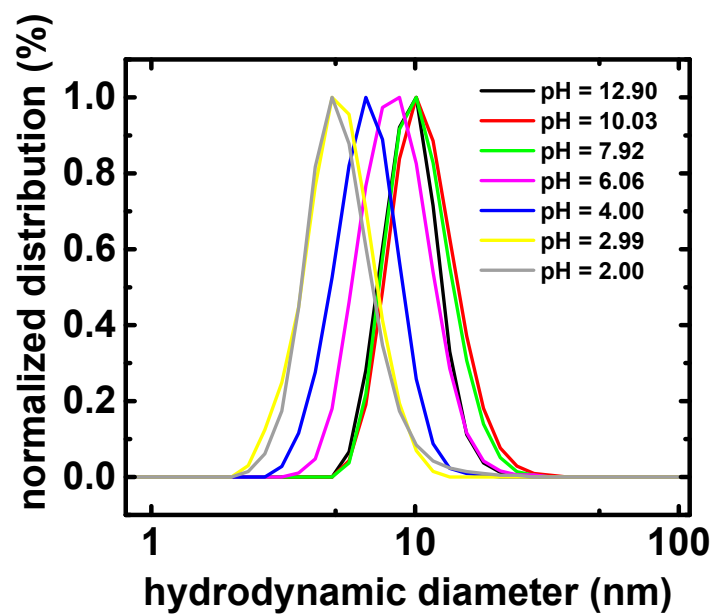


**Figure S22.** DLS hydrodynamic size distributions by volume of Rif-(P*t*BA-*b*-P*t*BA-Br)₃ in different pH.

**Table S1.** Calculation of Cu$^I$/Cu$^{II}$ ratio for the preparation of rifampicin-based macromolecules.

| Entry (according to Table 1) | $k_p{}^{app}$ (h$^{-1}$) [a] | $[P_n{}^\bullet]$ (M × 10$^{10}$) [a] | $K_{ATRP}$ (× 10$^8$) [b] | $[P_n\text{-Br}]$ (mM) | $[Cu^I]/[Cu^{II}]$ [c] | $[Cu^IL^+]$ (%) | $[Br\text{–}Cu^{II}L^+]$ (%) |
|---|---|---|---|---|---|---|---|
| 1 | 0.133 | 13.3 | 0.0047 | 1.35 | 0.02 | 2.1 | 97.9 |
| 2 | 0.109 | 10.9 | 1.30 | 2.71 | 31.06 | 96.9 | 3.1 |
| 3 | 0.095 | 9.53 | 1.30 | 2.71 | 27.07 | 96.4 | 3.6 |
| 4 | 0.137 | 13.3 | 1.30 | 6.74 | 15.18 | 93.8 | 6.2 |
| 5 | 0.097 | 9.42 | 1.30 | 1.95 | 37.17 | 97.4 | 2.6 |

[a] The radical concentration $[P_n{}^\bullet]$ was calculated according to the equation defined as $[P_n{}^\bullet] = \left(\frac{d\ln[M]}{dt}\right)(k_p)^{-1}$ [1], where $\frac{d\ln[M]}{dt}$ values were calculated from the first order kinetics plots (S8c in SI, 1a, 2a, 3a and 4a) [2], $k_p = 2.77 \times 10^4$ M$^{-1}$s$^{-1}$ for $n$BA polymerization [3], $k_p = 2.86 \times 10^4$ M$^{-1}$s$^{-1}$ for $t$BA polymerization [4], [b] entry 1: $K_{ATRP} = 4.7 \times 10^{-5}$ was determined theoretically for the CuI/TPMA$^+$ catalyst acetonitrile at 25°C [5]; entry 2–5: $K_{ATRP} = 1.3 \times 10^{-8}$ was determined for the Cu$^I$/TPMA$^+$ catalyst in methyl acrylate/acetonitrile 50/50 (v/v) at 50°C [6] [c] The Cu$^I$/Cu$^{II}$ ratio was calculated according to the equation defined as $\frac{[Cu^ITPMA^+]}{[Br\text{–}Cu^{II}TPMA^+]} = \frac{[P_n{}^\bullet]}{[P_n\text{–}Br]K_{ATRP}}$ [6].

**Table S2.** Theoretical Al$^{3+}$ concentration in solution and polymer by monomer conversion.

| Entry (according to Table 1 and S1) | Q [a] (C) | $n_{Al^{3+}}$ [b] (mol × 10$^5$) | $[Al^{3+}]_{solution}$ [c] (ppm by wt) | $[Al^{3+}]_{polymer}$ [d] (ppm by wt) |
|---|---|---|---|---|
| 1 | 12.93 | 4.47 | 48.9 | 11.7 |
| 2 | 16.53 | 5.71 | 98.6 | 25.1 |
| 3 | 16.53 | 5.71 | 98.6 | 26.3 |
| 4 | 21.06 | 7.28 | 128.0 | 48.9 |
| 5 | 12.85 | 4.44 | 87.8 | 25.8 |

[a] The total passed charge was calculated by integration of the chronoamperometry (CA) area ( $Q = I \cdot t$); [b] theoretical amount of Al$^{3+}$ in the reaction mixture was calculated from CA: $n_{Al^{3+}} = Q/F/3$ where $F = 96485$ C/mol; [c] the Al concentration in the reaction mixture was calculated according to the equation defined as: $[Al^{3+}]_{solution} = [Al^{3+}]$ MW$_{Al}$ / wt$_{total}$ × 1000000 where solution density was assumed as $(d) = d_{DMF} \cdot \% (v/v)_{DMF} + d_{monomer} \cdot \% (v/v)_{monomer}$; [d] the Al concentration in pure polymer sample was determined as follows: $[Al^{3+}]_{polymer} = [Al^{3+}]_{solution} / df \cdot$ conversion, where $df$ is dilute factor, $df = 2$ [7].

**Table S3.** Calculation of theoretical Dead Chain Fraction (DCF$_{theo}$) for polymerization of acrylates at low copper catalyst loading.

| Entry (according to Table 1) | $[P_n{}^\bullet]$ [a] (M × 10$^{10}$) | $[D]$ [b] (M × 10$^6$) | $[P_n\text{–}Br]$ (mM) | DCF$_{theo}$ [c] (%) |
|---|---|---|---|---|
| 1 | 13.3 | 3.52 | 1.35 | 0.26 |
| 2 | 10.9 | 3.30 | 2.71 | 0.12 |
| 3 | 9.53 | 2.51 | 2.71 | 0.09 |
| 4 | 13.3 | 6.37 | 6.74 | 0.09 |
| 5 | 9.42 | 3.52 | 1.95 | 0.18 |

[a] The radical concentration $[P^\bullet]$ was calculated according to the equation defined as $[P_n{}^\bullet] = \left(\frac{d\ln[M]}{dt}\right)(k_p)^{-1}$ [1], where $\frac{d\ln[M]}{dt}$ values were calculated from the first order kinetics plots (Figure 2a) [8], entry 1: $k_p = 2.86 \times 10^4$ M$^{-1}$s$^{-1}$ [4], entry 2-5: $k_p = 2.77 \times 10^4$ M$^{-1}$s$^{-1}$ [9]. [b] The concentration of terminated chains $[D]$ was calculated according to the equation defined as $[D] = k_t[P]^2 t$ where $t$ (denote reaction time) = 19800 s (entry 1), $t$ = 27601 s (entry 2 and 3), $t$ = 36000 s (entry 4) and $t$ = 39600 s (entry 5), $k_t = 1.0 \times 10^8$ M$^{-1}$s$^{-1}$ [10]. [c] DCF $= \left(\frac{[D]}{[P\text{–}X]_0}\right) \times 100\%$ [1].

**Table S4.** Results of the detaching of polymer arms from rifampicin-based macromolecules.

| Entry (according to Table 1) | $M_{n,theo}$ ($\times 10^{-3}$) [a] (chain) | $DP_{n,theo}$ [b] (chain) | $M_{n,app}$ ($\times 10^{-3}$) [c] (chain) | $DP_{n,app}$ [b] (chain) | $M_w/M_n$ [c] | $f_i$ [d] (%) |
|---|---|---|---|---|---|---|
| 4 | 9.9 | 77 | 23.4 | 182 | 1.20 | 42 |
| 5 | 23.6 | 184 | 44.6 | 348 | 1.42 | 53 |

[a] $M_{n,th}$ = ([$t$BA]$_0$/[Rif-Br$_3$]$_0$) × conversion × $M_{tBA}$, [$t$BA]$_0$—initial monomer concentration, [Rif-Br$_3$]$_0$—initiator concentration; [b] established according to Table 1; [c] apparent $M_n$ and $M_w/M_n$ of the arms cleaved from the rifampicin-based macromolecules determined by THF GPC (PS standards); [d] efficiency of initiation: $f_i$ = (DP$_{n,theo}$ (per chain)/DP$_{n,app}$ (per chain)) × 100%.

**Table S5.** Experimental values of contact angles, parameters of free surface energy (FSE) as calculated by Owens-Wendt method for rifampicin-based polymer coatings.

| Entry (according to Table 1) | Polymer | Experimental values of θ (°) | | | | Parameters of FSE (mJ/m²) water-diiodomethane | | |
|---|---|---|---|---|---|---|---|---|
| | | Diiodomethane | Standard deviation | Water | Standard deviation | $\gamma_s$ | $\gamma_s^d$ | $\gamma_s^p$ |
| 4 | P$t$BA | 58.36 | 2.63 | 90.06 | 1.93 | 29.82 | 26.94 | 2.88 |
| | PAA | 45.12 | 0.76 | 69.50 | 2.17 | 41.09 | 30.32 | 10.77 |
| 5 | P$t$BA | 70.64 | 1.30 | 92.34 | 0.96 | 23.54 | 19.55 | 3.99 |
| | PAA | 50.49 | 0.91 | 81.96 | 1.75 | 35.01 | 30.06 | 4.95 |

**Table S6.** Volume mean diameter of rifampicin-based macromolecules at varying pH.[a]

| Sample | pH | Hydrodynamic diameter (nm) |
|---|---|---|
| 1 | 12.90 | 14.59 ± 0.60 |
| 2 | 10.03 | 11.96 ± 0.80 |
| 3 | 7.92 | 11.48 ± 1.16 |
| 4 | 6.06 | 9.21 ± 1.35 |
| 5 | 4.00 | 6.96 ± 0.50 |
| 6 | 2.99 | 5.48 ± 0.84 |
| 7 | 2.00 | 5.70 ± 0.29 |

[a] The experiment was conducted for the polymer sample received according to Table 1, entry 5 after acidic hydrolysis.

## References

1. Zhong, M.; Matyjaszewski, K. How fast can a CRP be conducted with preserved chain end functionality? *Macromolecules* **2011**, *44*, 2668–2677, doi:10.1021/ma102834s.
2. Chmielarz, P.; Krys, P.; Wang, Z.; Wang, Y.; Matyjaszewski, K. Synthesis of well-defined polymer brushes from silicon wafers *via* surface-initiated *se*ATRP. *Macromol. Chem. Phys.* **2017**, *218*, 1700106, doi:10.1002/macp.201700106.
3. Buback, M.; Kurz, C.H.; Schmaltz, C. Pressure dependence of propagation rate coefficients in free-radical homopolymerizations of methyl acrylate and dodecyl acrylate. *Macromol. Chem. Phys.* **1998**, *199*, 1721–1727, doi:10.1002/(SICI)1521-3935(19980801)199:8<1721::AID-MACP1721>3.0.CO;2-5.
4. Dervaux, B.; Junkers, T.; Schneider-Baumann, M.; Du Prez, F.E.; Barner-Kowollik, C. Propagation rate coefficients of isobornyl acrylate, *tert*-butyl acrylate and 1-ethoxyethyl acrylate: A high frequency PLP-SEC study. *J. Polym. Sci. A Polym. Chem.* **2009**, *47*, 6641–6654, doi:10.1002/pola.23706.
5. Bortolamei, N.; Isse, A.A.; Di Marco, V.B.; Gennaro, A.; Matyjaszewski, K. Thermodynamic properties of copper complexes used as catalysts in atom transfer radical polymerization. *Macromolecules* **2010**, *43*, 9257–9267, doi:10.1021/ma101979p.

6. Wang, Y.; Kwak, Y.; Buback, J.; Buback, M.; Matyjaszewski, K. Determination of ATRP equilibrium constants under polymerization conditions. *ACS Macro Lett.* **2012**, *1*, 1367–1370, doi:10.1021/mz3005378.

7. Chmielarz, P. Synthesis of $\alpha$-D-glucose-based star polymers through simplified electrochemically mediated ATRP. *Polymer* **2016**, *102*, 192–198, doi: 10.1016/j.polymer.2016.09.007.

8. Chmielarz, P.; Fantin, M.; Park, S.; Isse, A.A.; Gennaro, A.; Magenau, A.J.D.; Sobkowiak, A.; Matyjaszewski, K. Electrochemically mediated atom transfer radical polymerization (*e*ATRP). *Prog. Polym. Sci.* **2017**, *69*, 47–78, doi:10.1016/j.progpolymsci.2017.02.005.

9. Buback, M.; Kurz, C.H.; Schmaltz, C. Pressure dependence of propagation rate coefficients in free-radical homopolymerizations of methyl acrylate and dodecyl acrylate. *Macromolecular Chemistry and Physics* **1998**, *199*, 1721–1727, doi:10.1002/(SICI)1521-3935(19980801)199:8<1721::AID-MACP1721>3.0.CO;2-5.

10. Barth, J.; Buback, M.; Hesse, P.; Sergeeva, T. Termination and transfer kinetics of butyl acrylate radical polymerization studied via SP-PLP-EPR. *Macromolecules* **2010**, *43*, 4023–4031, doi:10.1021/ma1006039.